

ARTICLE OPEN



Dopant-assisted stabilization of negatively charged single nitrogen-vacancy centers in phosphorus-doped diamond at low temperatures

Jianpei Geng ¹✉, Tetyana Shalomayeva ¹✉, Mariia Gryzlova¹, Amlan Mukherjee ¹, Santo Santonocito¹, Dzhavid Dzhavadzade¹, Durga Bhaktavatsala Rao Dasari ¹, Hiromitsu Kato ², Rainer Stöhr¹, Andrej Denisenko¹, Norikazu Mizuochi ^{3,4,5} and Jörg Wrachtrup¹

Charge state instabilities have been a bottleneck for the implementation of solid-state spin systems and pose a major challenge to the development of spin-based quantum technologies. Here we investigate the stabilization of negatively charged nitrogen-vacancy (NV^-) centers in phosphorus-doped diamond at liquid helium temperatures. Photoionization of phosphorous donors in conjunction with charge diffusion at the nanoscale enhances NV^0 to NV^- conversion and stabilizes the NV^- charge state without the need for an additional repump laser. The phosphorus-assisted stabilization is explored and confirmed both with experiments and our theoretical model. Stable photoluminescence-excitation spectra are obtained for NV^- centers created during the growth. The fluorescence is continuously recorded under resonant excitation to real-time monitor the charge state and the ionization and recombination rates are extracted from time traces. We find a linear laser power dependence of the recombination rate as opposed to the conventional quadratic dependence, which is attributed to the photo-ionization of phosphorus atoms.

npj Quantum Information (2023)9:110; <https://doi.org/10.1038/s41534-023-00777-7>

INTRODUCTION

Spin defects in wide-bandgap semiconductors^{1–3} are promising candidates for quantum information processing due to their excellent magneto-optical properties. The negatively charged nitrogen-vacancy (NV^-) center in diamond¹ has become a leading contender among these defects benefiting from efficient optical initialization and readout of the spin state^{4,5}, long spin coherence time⁶, and high-fidelity quantum control⁷. Substantial improvement has been achieved toward using these defects for spin-based quantum computation^{8,9}, simulation^{10,11}, nanoscale quantum sensing and imaging^{12–15}, and quantum networks^{16–19}. As only the negatively charged NV^- state is useful for the aforementioned applications, a key challenge is to continuously monitor its charge state and stabilize it. The stabilization of the NV^- charge state becomes even more important for shallow NV centers^{20,21} wherein sensitivity and spatial resolution get compromised in quantum sensing and imaging experiments^{22,23} due to charge instability. Usually, a repump mechanism is invoked using an additional laser to make sure that the defect remains in its correct charge state for further processing as shown in Fig. 1a and b. This additional check and the involved repump mechanisms have been a bottleneck and slow down the performance of these systems for cutting-edge industrial applications, and also increase the overhead in miniaturization trends. The use of a repump laser also causes spurious effects such as spectral diffusion²⁴ deteriorating the spin-photon interfaces²⁵ formed with these defects. Conventionally, this repump laser is used in between the operating pulses to bring the defect back to the correct charge state i.e., a conversion from the neutrally charged NV^0 to the negatively charged NV^- state^{26–28}. Here we overcome

this limitation by introducing dopants in the diamond lattice acting as electron donors thereby intrinsically assisting this charge state conversion without the need for external repump fields.

Among the various methods^{21,29–35} developed to control and stabilize the charge state of NV centers in diamond, a promising one is doping of electron donor impurities such as phosphorus^{32–35}. Previous studies of charge state dynamics of NV centers in phosphorus-doped diamond either used ensemble samples or room temperature experiments, where a relative NV^-/NV^0 population has been analyzed under the illumination of the green or orange laser. While these studies clearly indicate the charge state stabilization by photo-ionized electrons from the dopants, a clear distinction between this stabilization from that caused by a repump laser is not evident. This is due to the fact that the excitation lasers used in their experiment can also cause the $\text{NV}^0 - \text{NV}^-$ transition alongside those caused by the photoionized electrons. Hence a quantitative description through its experimental verification of how the phosphorus impurities stabilize the NV^- charge state at the level of a single center is essential to understand the physical mechanism leading to such charge stabilization. Exploring these effects at low temperatures of 4 K opens up the venue for its application in a large number of quantum protocols. For this, we here monitor the charge-state dynamics under resonant excitation for NV centers in phosphorus-doped diamond at cryogenic temperatures and show how the photo-ionization of the phosphorous donors affects the recombination/transition rates among the charge states and explore the differences from the repump mechanism using a repump-laser.

In this letter, we investigate the charge state stability of NV^- centers in phosphorus-doped diamond under resonant excitation

¹3rd Institute of Physics, ZAQuant, University of Stuttgart, 70569 Stuttgart, Germany. ²National Institute of Advanced Industrial Science and Technology (AIST), Tsukuba, Ibaraki 305-8568, Japan. ³Institute for Chemical Research, Kyoto University, Gokasho, Uji, Kyoto 611-0011, Japan. ⁴Center for Spintronics Research Network, Kyoto University, Uji, Kyoto 611-0011, Japan. ⁵International Center for Quantum-field Measurement Systems for Studies of the Universe and Particles (QUP), KEK, Tsukuba, Ibaraki 305-0801, Japan.

✉email: jianpei.geng@pi3.uni-stuttgart.de; tetyana.shalomayeva@pi3.uni-stuttgart.de

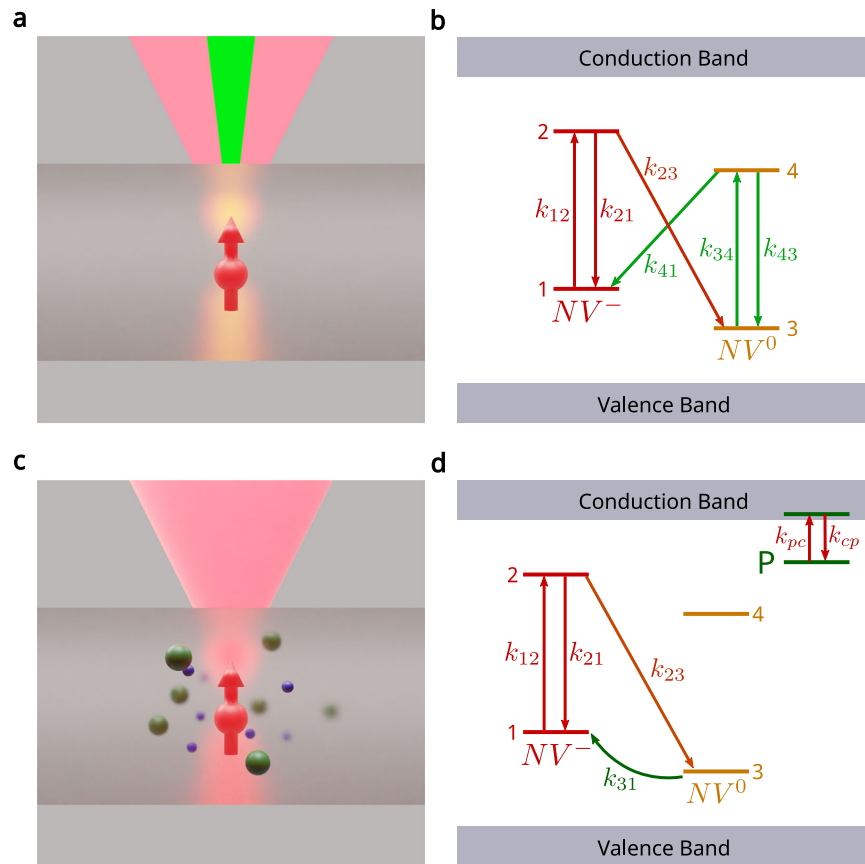


Fig. 1 Charge state conversion of NV center in diamond. **a** Schematic representation of the conventional method to keep the NV center in NV^- with repump laser. The red sphere with an arrow represents the NV center in diamond. The red and green cones represent the illumination of the red resonant and additional repump lasers respectively. **b** Illustration of the NV photo- and charge dynamics under the illumination of the resonant and repump lasers. The red solid lines with arrows indicate the population transfer of the NV state due to the resonant laser, which ultimately ionizes the NV center into NV^0 . The green solid lines with arrows indicate the recombination pathway of population transfer provided by the repump laser. **c** Schematic representation of NV^- charge state stabilization assisted by photo-ionization of phosphorus impurities. The red sphere with an arrow represents the NV center in diamond. The red cone represents the illumination of the red laser resonant to the NV^- excitation. The green spheres show phosphorus impurities. The blue spheres represent electrons created by the photo-ionization of the phosphorus impurities. **d** Illustration of the photo- and charge dynamics of the NV center in phosphorus-doped diamond under the illumination of the resonant laser. The energy levels of both the NV center and the phosphorus impurity are presented. The red solid lines with arrows indicate the photo-ionization of the NV center and the phosphorus impurity due to the resonant laser excitation. The green solid line indicates the recombination pathway provided by capturing the electrons created by the photo-ionization of the phosphorus impurities.

at liquid helium temperatures and reveal the key role of photo-ionization of phosphorus impurities in the charge-state stabilization of the defect. Consequently, stable photoluminescence-excitation (PLE) spectra of NV^- centers created during the growth process are obtained without any repump laser. This enables us to realize real-time monitoring of the NV charge state by recording fluorescence under 636 nm resonant excitation. Ionization and recombination rates of the NV centers are extracted from time traces of the fluorescence at various excitation powers. Further, the linear power dependence of the recombination rate was observed, distinguished from the well-known quadratic dependence²⁶ for NV centers in the intrinsic diamond when a repump laser is applied. This linear power dependence could be attributed to the dependence of the photo-ionization-induced carrier density on the laser power. Finally, a theoretical model is developed to gain insight into the charge state stabilization of NV centers assisted by photo-ionization of the phosphorus impurities, which is helpful in the optimization of phosphorus concentration to realize stable and narrow PLE spectra of NV^- centers created during the growth process.

RESULTS

Experiment

The measurements were performed on NV centers in a phosphorus-doped diamond with a home-built cryogenic confocal setup. The phosphorus-doped layer was epitaxially grown onto Ib-type (111)-oriented diamond substrate by CVD with phosphorus concentration of 5×10^{16} atoms cm^{-3} . NV centers created during growth could be found in the phosphorus-doped layer. Additional NV centers were created by implantation of $^{15}\text{N}^+$ ions in the phosphorus-doped layer with an energy of 9.8 keV and a dose of 1.3×10^{10} atoms cm^{-2} . Arrays of nanopillars³⁶ with apex sizes of 400, 450, and 500 nm were fabricated to enhance the photon collection efficiency of NV centers created by ion implantation. The NV centers created during growth and those created by ion implantation could be distinguished from their position, depth, and from the hyperfine spectrum seen in the ODMR signal. We performed measurements on both types of NV centers for comparison and to gain deep insight into the role of phosphorus impurities in the NV spin and charge-state properties. The average spin coherence (Hahn Echo) time at liquid helium temperatures was measured to be (i) $T_2 = 1.94$ ms for NV centers

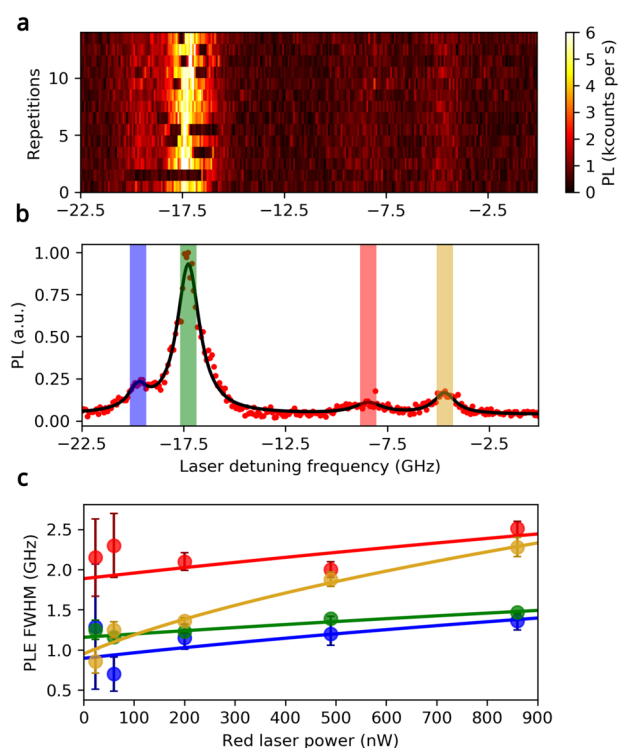


Fig. 2 Stable PLE spectrum of an NV center created during growth in the phosphorus-doped diamond. **a** PL intensity as a function of laser detuning (detuned from 636.60 nm) in several individual repetitions without repumping. Sharp changes in the PL intensity indicate NV ionization or recombination events. The measurements show a stable but broad PLE spectrum of NV^- over multiple repetitions. **b** PLE spectrum averaged over multiple repetitions in **a**. The circles are experimental data and the solid line is fit with a multi-Lorentz function. Blue, green, red, and yellow marked regions correspond to 4 different observed peaks. **c** Resonant laser power dependence of PLE full width at half maximum (FWHM). The circles with error bars represent the FWHMs obtained by fitting the PLE spectra at various laser powers. The error bars are from fitting and indicate the 95% confidence interval. Colors represent the FWHM values for each individual peak in **b** respectively. The fit of the laser power dependence of FWHM is shown by solid lines.

created during growth and (ii) $T_2 = 11.53 \mu\text{s}$ for those created by ion implantation. The long spin coherence time of NV centers created during growth is attributed to the suppression of paramagnetic vacancy complexes due to their charging by phosphorus atoms³⁴. Further details on the experimental setup, sample preparation, and spin coherence time measurements are given in Supplementary Note 1–3 and Supplementary Figs. 1 and 2 of the Supplementary Information.

Figure 2 shows the PLE measurements of an NV center created during the growth in a phosphorus-doped diamond at liquid helium temperature. The measurements were performed by recording the fluorescence while sweeping the laser frequency across the NV^- resonance (637 nm). A peak in the PLE spectrum is observed when the NV^- center gets resonantly excited. However, since the resonant excitation could photo-ionize NV^- into NV^0 and not excite NV^0 back into NV^- ³⁷, the NV center would essentially stay in NV^0 charge state leading to the disappearance of the PLE peak. A recombination pathway from NV^0 to NV^- requires an additional electron which becomes available by an additional laser i.e., optical repumping either with a 488 nm³⁷, 532 nm²⁴, or 575 nm laser²⁷. On the other hand, as shown in Fig. 2a we observe a stable PLE spectrum of the NV^- center even in the absence of the repump laser. Disappearance and recovery of fluorescence could

be observed in a single PLE scan when the laser frequency is swept across a resonant transition while still being within the linewidth estimated with other PLE scans. Also observed is the disappearance and recovery of fluorescence at the resonant transition during the repetitions. The disappearance of fluorescence indicates the ionization of NV^- into NV^0 , and the fluorescence recovery indicates the recombination of NV^0 to NV^- . Due to this continuous ionization and recombination processes, we observe a stable PLE spectrum of all measured NV centers created during growth in the phosphorus-doped layer of diamond without the need for a repump laser (see Supplementary Note 4 and Supplementary Fig. 3 of the Supplementary Information). This clearly indicates that a recombination pathway has been provided by the phosphorus impurities.

Phosphorus is a shallow electron donor in diamond with an energy level located at 0.57 eV below the conduction band edge^{38,39}, and thus could be photo-ionized by the 636 nm laser used in the PLE measurements. Electrons created by photo-ionization of the phosphorus impurities could be captured by NV^0 , providing the recombination pathway. Figure 2b shows the PLE spectrum of an NV^- center averaged over multiple repetitions, which is fitted by a multi-Lorentz function. The PLE spectrum shows four peaks. By comparing the four resonant frequencies with calculation from the NV^- Hamiltonian^{1,40,41}, we attribute the peaks to the transitions from the NV^- ground to excited states with a transverse strain of about 4.5 GHz (see Supplementary Note 5 and Supplementary Fig. 5 of the Supplementary Information). At this transverse strain the spin mixing between $|m_s = 0\rangle$ and $|m_s = \pm 1\rangle$ in the excited state is negligible, and only a single transition from the ground-state $|m_s = 0\rangle$ or $|m_s = \pm 1\rangle$ should be observed for each excited-state level. Due to the large PLE linewidth in order of 1 GHz, two pairs of transitions are overlapped and could not be distinguished from each other in the PLE measurements, and four PLE peaks are experimentally observed. The linewidth of the PLE peaks is much broader than the Fourier transform limited linewidth of NV centers in intrinsic diamond⁴². The broadening is attributed to the environmental charge fluctuation induced by photo-ionized electrons of the phosphorus impurities. We measured PLE spectra at various excitation powers (see Supplementary Note 5 and Supplementary Fig. 4 of the Supplementary Information) and various laser polarizations (see Supplementary Note 7 and Supplementary Fig. 7 of the Supplementary Information), and the power dependence of the PLE linewidths is shown in Fig. 2c.

The charge dynamics of the NV centers that are created during growth are investigated under the resonant excitation of a 636 nm laser. We would like to note that at this frequency only the NV^- charge state is excited but not the NV^0 i.e., fluorescence from the NV center can be detected only when it is in the NV^- charge state. Therefore, the charge state could be real-time monitored by recording the fluorescence. If the excitation is spin selective, driving the spin transitions in the NV^- ground state by an appropriate microwave field would suppress any spin polarization⁵ and maintain the NV^- fluorescence. In our experiment, a microwave drive was not necessary, because all the spin levels could be simultaneously excited by a single excitation as the PLE lines are quite broad. Figure 3a shows a typical time trace of the fluorescence where the resonant excitation power is chosen to be 148 nW. The high count level indicates the NV center in NV^- charge state and the low level is the background counts with the NV center in NV^0 . As we can see, the NV center stays for a much shorter time in NV^0 than in NV^- , corresponding to a larger recombination rate than the ionization rate. The intensity histogram of the time trace is presented in Fig. 3b, showing a relatively larger population of NV^- than the NV^0 charge state. The histogram is fitted with the function derived by Shields et al.⁴³, in which the photon count distribution is described by count rates for NV^- and NV^0 charge states together with the ionization and

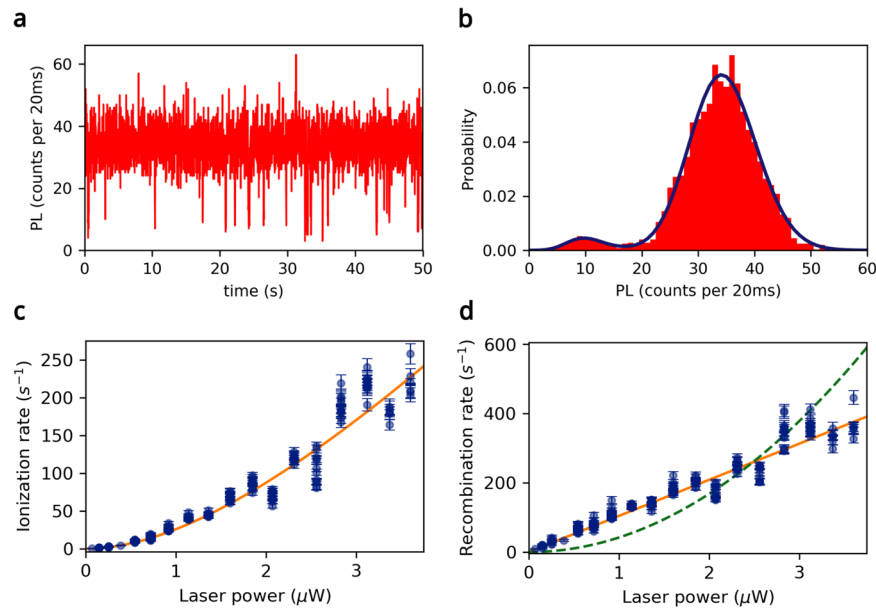


Fig. 3 Experimental charge dynamics at various laser powers of an NV center created during growth in the phosphorus-doped diamond. **a** Time trace of the fluorescence under continuous illumination of 148 nW, 636 nm resonant laser. Blinking events arise from dynamic NV charge ionization and recombination. **b** Histogram of **a**, showing a larger population of NV^- (right peak) than NV^0 (left peak). The solid line is a fit. **c** Laser power dependence of ionization rate. The circles represent experimental data and the solid line is a fit with a saturation-modified quadratic function. The saturation power is fixed as $4.5 \mu W$ in the fitting. **d** Laser power dependence of recombination rate. The circles are experimental data and the solid line is a linear fit according to the model. For comparison, the dashed line is a quadratic fit according to the laser power dependence for NV centers in the non-doped diamond. Each experimental data in **c** and **d** is obtained by measuring the time trace and fitting the histogram at corresponding laser power. At each laser power various time-trace measurements are performed and similar but different values of the rates are obtained. The error bars on the experimental data are from fitting and indicate the 95% confidence interval.

recombination rates determining the charge-state switching. A set of distributions of the photon count within various counting times from the same time trace is fitted to improve the fitting precision of the rates (see Supplementary Note 8 and Supplementary Fig. 8 of the Supplementary Information). The fitting result is shown as the solid line in Fig. 3b, which gives an ionization rate of $k_{ion} = 0.5(1) s^{-1}$ and a recombination rate of $k_{rec} = 11(3) s^{-1}$, and thus an NV^- population of $P_- = k_{rec}/(k_{ion} + k_{rec}) = 96(2)\%$. The time traces of fluorescence are recorded at various excitation powers, and corresponding photon count distributions are fitted to extract the rates. Figure 3c and d show the excitation power dependence of the ionization and recombination rate, respectively. The ionization rate could be well fitted with function $k_{ion} = aP_L^2/(1 + P_L/P_s)$, where P_L is the excitation power, P_s is the saturation power, and a is a fitting coefficient. The good agreement of the numerical fit to the obtained experimental data indicates a two-photon process of the photo-ionization of NV^- , which is consistent with previous research^{26,27}. However, the recombination rate shows a linear excitation power dependence which is in contrast to the previous observations²⁶ where a similar two-photon excitation pathway has been known. Measurements on several various NV centers give consistent linear excitation power dependence of the recombination rates (see Supplementary Note 9 and Supplementary Fig. 9 of the Supplementary Information). This linear dependence could be attributed to the additional electrons provided by the photoionized phosphorus atoms, and in the following, we present a simple model to explain this power dependence.

Model

As mentioned before, the resonant excitation is absorbed only by NV^- and hence alone cannot contribute to the recombination

pathway from NV^0 to NV^- . Therefore, the recombination pathway could only be provided by the electrons from the donor impurities. The laser power dependence of the recombination rate indicates the interplay of the laser intensity and the concentration of phosphorus impurities. Photoconductivity studies of photoionized phosphorus impurities in diamond^{44,45} have clearly shown dependence on the excitation laser and impurity concentration. From these studies and our experimental observations, we develop below a simple model to extract the recombination rate and its dependence on the above-mentioned parameters.

As illustrated in Fig. 1c, we consider phosphorus impurities within the focal volume of the NV center excitation. The phosphorus concentration of $5 \times 10^{16} cm^{-3}$ gives a number of about 5×10^4 phosphorus atoms in the focal volume of roughly $1 \mu m^3$, which is much larger than the number of NV center since the measurements are on single NV centers. Therefore, we neglect the influence of the NV charge dynamics on the charge dynamics of the phosphorus impurities and only consider the opposite one. Photo-ionized electrons created by the photo-ionization of the impurities could diffuse spatially and get captured by the NV center to convert it from NV^0 to NV^- . The spatial power distribution of the laser (beam profile) can be described as

$$I(\mathbf{r}) = P_L f(\mathbf{r}), \quad (1)$$

where P_L is the laser power, $f(\mathbf{r})$ is the normalized intensity distribution satisfying $\int f(\mathbf{r}) dS = 1$, and $I(\mathbf{r})$ is the laser intensity at position \mathbf{r} . The photo-ionization of the phosphorus impurity is modeled with the transition of the electron from the phosphorus level to the conduction band, as is shown in Fig. 1d. The transition rate k_{pc} is proportional to the laser intensity, and is thus a function of \mathbf{r} ,

$$k_{pc}(\mathbf{r}) = aI(\mathbf{r}), \quad (2)$$

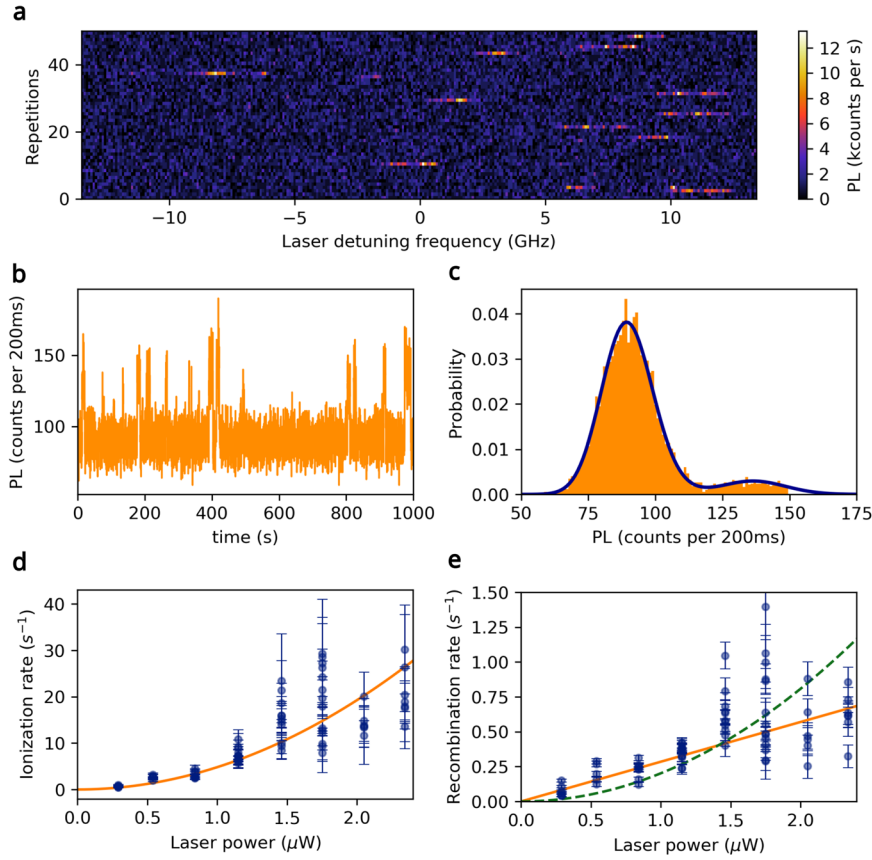


Fig. 4 PLE spectrum and charge dynamics of an NV center created by ion implantation in the phosphorus-doped diamond. **a** PL intensity as a function of laser detuning (detuned from 636.6 nm) in several individual repetitions without repumping. Unstable resonant excitation is observed only at certain individual repetitions, indicating the NV center in NV^0 charge state most of the time. **b** Time trace of the fluorescence of the NV center under continuous illumination with 290 nW, 594 nm laser, showing NV^- charge state with higher counts and NV^0 with lower counts. **c** Histogram of **b**, showing a larger population of NV^0 (left peak) than NV^- (right peak). The solid line is a fit. **d** Laser power dependence of ionization rate. The circles represent experimental data and the solid line is a fit with a saturation-modified quadratic function. Each circle corresponds to an individual measurement. **e** Laser power dependence of recombination rate. The circles are experimental data and the solid line is a linear fit according to the model. For comparison, the dashed line is a quadratic fit according to the laser power dependence for NV centers in the non-doped diamond. Each experimental data in **d** and **e** is obtained by measuring the time trace and fitting the histogram at corresponding laser power. At each laser power various time-trace measurements are performed and similar but different values of the rates are obtained. The error bars on the experimental data are from fitting and indicate the 95% confidence interval.

where α is determined by the photo-ionization cross-section of phosphorous atoms in a diamond lattice. The rate of the electron transition from the conduction band back to the phosphorus level is denoted as k_{cp} . We can now estimate the population of the electron in the conduction band due to the photo-ionization of a phosphorus impurity at position \mathbf{r} as

$$P_e(\mathbf{r}) = \frac{k_{pc}(\mathbf{r})}{k_{pc}(\mathbf{r}) + k_{cp}}. \quad (3)$$

The electron density n_e at the position of the NV center due to diffusion of the electrons created by photo-ionization of the phosphorus impurities can be written as

$$n_e = \int \eta(\mathbf{r}) P_e(\mathbf{r}) n_p dV, \quad (4)$$

where n_p is the phosphorus concentration, and $\eta(\mathbf{r})$ is the probability that an electron in the conduction band at position \mathbf{r} diffuses into a unit volume at the position of the NV center. We assume a homogeneous phosphorus concentration n_p for simplicity. $\eta(\mathbf{r})$ is dependent on the electron diffusion constant and lifetime due to capture by impurities. The capture of electrons by the NV^0 center gives the NV recombination rate

$$k_{rec} = \kappa n_e, \quad (5)$$

where κ is the electron capture coefficient of NV^0 . With Eq. (1)–(5), k_{rec} could be derived as

$$k_{rec} = \kappa \alpha \int \frac{\eta(\mathbf{r}) f(\mathbf{r})}{\alpha P_L f(\mathbf{r}) + k_{cp}} dV n_p P_L. \quad (6)$$

The linear laser power dependence of the recombination rate would be immediately obtained if the laser power is small, i.e. $\alpha P_L f(\mathbf{r}) \ll k_{cp}$, which gives

$$k_{rec} = \kappa \frac{\alpha}{k_{cp}} \int \eta(\mathbf{r}) f(\mathbf{r}) dV n_p P_L, \quad (7)$$

consistent with the experimental results.

The model is further confirmed with measurements on NV centers created by ion implantation in the phosphorus-doped diamond. The implantation could create a large number of impurities such as vacancy-complex. The impurities play the role of either electron traps or electron acceptors which capture electrons from the valance band and create holes under the laser illumination. In each case, the probability $\eta(\mathbf{r})$ decreases due to the trap or combination of the electrons by the impurities or holes. According to Eq. (7), this causes a decrease in the recombination rate but doesn't change the linear laser power dependence. We performed PLE measurements on multiple NV centers created by ion implantation without repump laser. For many of them, the PLE

spectra weren't detectable. For others, PLE peaks are observable only in certain repetitions as shown in Fig. 4a. In most repetitions of the PLE scan, the NV centers are in a dark state. These measurements indicate a much smaller recombination rate of NV centers created by ion implantation than those created during growth, which are further confirmed by the comparison of NV⁻ population between the two types of NV centers (see Supplementary Note 10 and Supplementary Fig. 10 of the Supplementary Information) and by measurements of excitation power dependence of the total charge-dynamics rate of the NV center created by ion implantation under illumination of green and orange lasers (see Supplementary Note 11 and 12 and Supplementary Figs. 11 and 12 of the Supplementary Information). Real-time monitoring of the charge state of these NV centers by recording fluorescence under resonant excitation becomes challenging due to the too small recombination rates. That's why we real-time monitor the charge state with 594 nm excitation. A typical time trace of the fluorescence and its histogram is shown in Fig. 4b, c, where a small but non-zero NV⁻ population is observed. The extracted ionization and recombination rate as a function of laser power is shown in Fig. 4d, e, respectively. The ionization rate shows a quadratic power dependence, and the recombination rate could be fitted with a linear function of the laser power. These results coincide with the expectation from the model.

DISCUSSION

While the photo-ionized electrons have a positive impact on the recombination rate they on the other hand could have a negative effect on the optical linewidth due to increased electric noise. Counterintuitively we have found that the line width is insensitive to the applied power of the resonant laser (Fig. 2c), and remained little changed for increasing laser power up to a μW . This counterintuitive effect can be understood only upon properly evaluating the electric field noise taking into consideration the screening effects caused by the photo-ionized free charge carriers. Using the Thomas-Fermi model for free electron gas at low temperatures we find the electron density dependence of the screening length and further the modified electric field (see Supplementary Note 6 and Supplementary Fig. 6 of the Supplementary Information for more details). We find that the electric field shows a linear increase with increasing electron density n_e when n_e is small, and an exponential decay when n_e is large. At a certain value of n_e the electric field reaches a maximum and remains almost unchanged for a considerable change of the electron density n_e near this value. From our experimental measurements, we conclude that we are in such a field-insensitive regime, from which we obtain the mean typical electron density to be $\sim 10^{10}\text{--}10^{14}\text{ cm}^{-3}$. This is in line with the actual phosphorous concentration of 10^{16} cm^{-3} , and assuming that not all the phosphorous dopants are ionized as explained above, an almost unchanged PLE linewidth dependence on the laser power can be understood.

Several protocols could be implemented to reduce the PLE linewidth. Since the electric field on the NV center caused by photo-ionization of phosphorus impurities would decrease with increasing electron density n_e due to screening effect, a straightforward method to reduce the linewidth would be to increase the electron density. This could be realized by increasing the laser power to improve the photo-ionization of phosphorus impurities. However, increasing laser power would also increase the NV ionization rate, leading to a decreased population of NV⁻ charge state. In addition, a large laser power could still lead to a large linewidth due to power broadening. To avoid these drawbacks, the excitation of NV center and photo-ionization of phosphorus impurities should be separated from each other. An available protocol would be to use an additional infrared laser to photo-ionize phosphorus impurities, since the NV center could not

be excited by the infrared laser. In this case, the PLE and charge dynamics measurements could be implemented with minimum power of red laser to keep small power broadening and NV ionization rate, while strong infrared laser could be continuously applied to ionize phosphorus impurities to reach a large electron density n_e for a large NV recombination rate and screening effect. Another protocol would be spatial separation of the NV center and phosphorus impurities, which is possible by growth of a phosphorus layer on intrinsic diamond with delta-doping⁴⁶. An electric field could be applied to control the spatial distribution of the electron density n_e . With these protocols reduced PLE linewidth could be expected.

In conclusion, we report PLE and charge-state measurements on single NV centers in phosphorus-doped diamond at 4 K. Stable PLE spectra without a repump laser, and a near unity probability to find the ingrown NV center in its correct charge state (NV⁻) under resonant excitation are observed. A linear excitation power dependence of the recombination rate is observed on NV centers created during growth clearly distinguishing the dopant-assisted recombination pathway from the laser-assisted process. For defect centers created by ion implantation, while no stable PLE spectrum could be observed, a recombination pathway from NV⁰ to NV⁻ (with low probability) is observed due to the presence of phosphorus impurities. Here once again a linear laser power dependence of the recombination rate is detected indicating a dopant-assisted recombination process. A simple model is developed to briefly describe various dependencies of the recombination rate on the laser and the dopant concentration. Further optimization of phosphorus concentration for stable and narrow PLE spectrum could be advantageous for quantum network applications as it removes the necessity of time-consuming repump which might enhance entanglement rates substantially^{18,19}.

METHODS

Experimental setup

The measurements were performed with a home-built cryogenic confocal microscope. The phosphorus-doped diamond with a phosphorus concentration of $5 \times 10^{16}\text{ cm}^{-3}$ was mounted inside a Janis ST-500 cold finger Helium flow cryostat at 4 K. The chamber was evacuated to 10^{-8} mbar. The lasers for excitation and phonon-sideband fluorescence from the NV centers went through the same air objective (Nikon LU Plan Fluor 100 \times , NA0.9). Each laser passed through an acousto-optic modulator (AOM) twice for pulse generation before going into the objective. The fluorescence was separated from the excitation lasers with a dichroic mirror and a 660–800 nm bandpass filter, and then detected by Perkin-Elmer avalanche photodiodes (APDs). More details about the experimental setup could be found in Supplementary Note 1 and Supplementary Fig. 1 of the Supplementary Information.

DATA AVAILABILITY

Data supporting the findings of this study are available within the article and its Supplementary information and from the corresponding authors upon request. Source data for reproducing the figures in the main text are available with the link <https://doi.org/10.18419/darus-3734>.

CODE AVAILABILITY

The code generated in this work is available from the corresponding authors upon reasonable request.

Received: 27 April 2023; Accepted: 13 October 2023;
Published online: 27 October 2023

REFERENCES

- Doherty, M. W. et al. The nitrogen-vacancy colour centre in diamond. *Phys. Rep.* **528**, 1–45 (2013).
- Christle, D. J. et al. Isolated electron spins in silicon carbide with millisecond coherence times. *Nat. Mater.* **14**, 160–163 (2015).
- Chejanovsky, N. et al. Single-spin resonance in a van der Waals embedded paramagnetic defect. *Nat. Mater.* **20**, 1079–1084 (2021).
- Neumann, P. et al. Single-shot readout of a single nuclear spin. *Science* **329**, 542–544 (2010).
- Robledo, L. et al. High-fidelity projective read-out of a solid-state spin quantum register. *Nature* **477**, 574–578 (2011).
- Balasubramanian, G. et al. Ultralong spin coherence time in isotopically engineered diamond. *Nat. Mater.* **8**, 383–387 (2009).
- Rong, X. et al. Experimental fault-tolerant universal quantum gates with solid-state spins under ambient conditions. *Nat. Commun.* **6**, 8748 (2015).
- Neumann, P. et al. Quantum register based on coupled electron spins in a room-temperature solid. *Nat. Phys.* **6**, 249–253 (2010).
- Abobeih, M. et al. Fault-tolerant operation of a logical qubit in a diamond quantum processor. *Nature* **606**, 884–889 (2022).
- Wu, Y. et al. Observation of parity-time symmetry breaking in a single-spin system. *Science* **364**, 878–880 (2019).
- Randall, J. et al. Many-body-localized discrete time crystal with a programmable spin-based quantum simulator. *Science* **374**, 1474–1478 (2021).
- Maze, J. R. et al. Nanoscale magnetic sensing with an individual electronic spin in diamond. *Nature* **455**, 644–647 (2008).
- Balasubramanian, G. et al. Nanoscale imaging magnetometry with diamond spins under ambient conditions. *Nature* **455**, 648–651 (2008).
- Shi, F. et al. Single-protein spin resonance spectroscopy under ambient conditions. *Science* **347**, 1135–1138 (2015).
- Song, T. et al. Direct visualization of magnetic domains and moiré magnetism in twisted 2d magnets. *Science* **374**, 1140–1144 (2021).
- Togan, E. et al. Quantum entanglement between an optical photon and a solid-state spin qubit. *Nature* **466**, 730–734 (2010).
- Bernien, H. et al. Heralded entanglement between solid-state qubits separated by three metres. *Nature* **497**, 86–90 (2013).
- Pompili, M. et al. Realization of a multinode quantum network of remote solid-state qubits. *Science* **372**, 259–264 (2021).
- Hermans, S. et al. Qubit teleportation between non-neighbouring nodes in a quantum network. *Nature* **605**, 663–668 (2022).
- Bluvstein, D., Zhang, Z. & Jayich, A. C. B. Identifying and mitigating charge instabilities in shallow diamond nitrogen-vacancy centers. *Phys. Rev. Lett.* **122**, 076101 (2019).
- Janitz, E. et al. Diamond surface engineering for molecular sensing with nitrogen-vacancy centers. *J. Mater. Chem. C* **10**, 13533–13569 (2022).
- Taylor, J. M. et al. High-sensitivity diamond magnetometer with nanoscale resolution. *Nat. Phys.* **4**, 810–816 (2008).
- Rugar, D. et al. Proton magnetic resonance imaging using a nitrogen-vacancy spin sensor. *Nat. Nanotechnol.* **10**, 120–124 (2015).
- Robledo, L., Bernien, H., Weperen, I. V. & Hanson, R. Control and coherence of the optical transition of single nitrogen vacancy centers in diamond. *Phys. Rev. Lett.* **105**, 177403 (2010).
- Faraon, A., Santori, C., Huang, Z., Acosta, V. M. & Beausoleil, R. G. Coupling of nitrogen-vacancy centers to photonic crystal cavities in monocrystalline diamond. *Phys. Rev. Lett.* **109**, 033604 (2012).
- Aslam, N., Waldherr, G., Neumann, P., Jelezko, F. & Wrachtrup, J. Photo-induced ionization dynamics of the nitrogen vacancy defect in diamond investigated by single-shot charge state detection. *N. J. Phys.* **15**, 013064 (2013).
- Siyushev, P. et al. Optically controlled switching of the charge state of a single nitrogen-vacancy center in diamond at cryogenic temperatures. *Phys. Rev. Lett.* **110**, 167402 (2013).
- Wirtsch, D. et al. Exploiting ionization dynamics in the nitrogen vacancy center for rapid, high-contrast spin, and charge state initialization. *Phys. Rev. Res.* **5**, 013014 (2023).
- Hauf, M. et al. Chemical control of the charge state of nitrogen-vacancy centers in diamond. *Phys. Rev. B* **83**, 081304 (2011).
- Grotz, B. et al. Charge state manipulation of qubits in diamond. *Nat. Commun.* **3**, 729 (2012).

- Doi, Y. et al. Deterministic electrical charge-state initialization of single nitrogen-vacancy center in diamond. *Phys. Rev. X* **4**, 011057 (2014).
- Groot-Berning, K. et al. Passive charge state control of nitrogen-vacancy centres in diamond using phosphorous and boron doping. *Phys. Status Solidi A* **211**, 2268–2273 (2014).
- Doi, Y. et al. Pure negatively charged state of the NV center in n-type diamond. *Phys. Rev. B* **93**, 081203 (2016).
- Herbschleb, E. et al. Ultra-long coherence times amongst room-temperature solid-state spins. *Nat. Commun.* **10**, 3766 (2019).
- Watanabe, A. et al. Shallow NV centers augmented by exploiting n-type diamond. *Carbon* **178**, 294–300 (2021).
- Momenzadeh, S. A. et al. Nanoengineered diamond waveguide as a robust bright platform for nanomagnetometry using shallow nitrogen vacancy centers. *Nano Lett.* **15**, 165–169 (2015).
- Beha, K., Batalov, A., Manson, N. B., Bratschitsch, R. & Leitenstorfer, A. Optimum photoluminescence excitation and recharging cycle of single nitrogen-vacancy centers in ultrapure diamond. *Phys. Rev. Lett.* **109**, 097404 (2012).
- Nesládek, M. et al. Low-temperature spectroscopic study of n-type diamond. *Phys. Rev. B* **59**, 14852 (1999).
- Sque, S., Jones, R., Goss, J. & Briddon, P. Shallow donors in diamond: chalcogens, pnictogens, and their hydrogen complexes. *Phys. Rev. Lett.* **92**, 017402 (2004).
- Batalov, A. et al. Low temperature studies of the excited-state structure of negatively charged nitrogen-vacancy color centers in diamond. *Phys. Rev. Lett.* **102**, 195506 (2009).
- Doherty, M. W., Manson, N. B., Delaney, P. & Hollenberg, L. C. The negatively charged nitrogen-vacancy centre in diamond: the electronic solution. *N. J. Phys.* **13**, 025019 (2011).
- Tamarat, P. et al. Stark shift control of single optical centers in diamond. *Phys. Rev. Lett.* **97**, 083002 (2006).
- Shields, B. J., Unterreithmeier, Q. P., de Leon, N. P., Park, H. & Lukin, M. D. Efficient readout of a single spin state in diamond via spin-to-charge conversion. *Phys. Rev. Lett.* **114**, 136402 (2015).
- Haenen, K. et al. Low temperature photoconductivity detection of phosphorus in diamond. *Phys. Status Solidi A* **174**, 53–58 (1999).
- Remes, Z. et al. Photo-hall measurements on phosphorus-doped n-type CVD diamond at low temperatures. *Phys. Status Solidi A* **199**, 82–86 (2003).
- Ohno, K. et al. Engineering shallow spins in diamond with nitrogen delta-doping. *Appl. Phys. Lett.* **101**, 082413 (2012).

ACKNOWLEDGEMENTS

We acknowledge financial support by European Union's Horizon 2020 research and innovation program AMADEUS under grant No. 101080136, Federal Ministry of Education and Research (BMBF) project MiLiQuant, Quamapolis, and Cluster4Future-QSens, as well as SPINNING under grant No.13N16219. N.M. would like to acknowledge the support by JSPS KAKENHI (21H04653), MEXT Q-LEAP (JPMXS0118067395), the Collaborative Research Program of Institute for Chemical Research, Kyoto University (2022-72), and the Spintronics Research Network of Japan.

AUTHOR CONTRIBUTIONS

J.G. and T.S. contributed equally to this work. J.W., R.S., and J.G. designed the experiment. J.G., T.S., M.G., A.M., and D.D. conducted the experiment. J.G. and T.S. analyzed the data with support from M.G. J.G., T.S., and D.B.R.D. developed the model. J.G. made the numerical simulation. N.M. and H.K. prepared the phosphorus-doped diamond sample. A.D. and S.S. made the ion implantation. R.S. created the nanopillars. J.G., T.S., and D.B.R.D. wrote the manuscript. All authors discussed the data, commented on the manuscript, and contributed to the paper.

FUNDING

Open Access funding enabled and organized by Projekt DEAL.

COMPETING INTERESTS

The authors declare no competing interests.

ADDITIONAL INFORMATION

Supplementary information The online version contains supplementary material available at <https://doi.org/10.1038/s41534-023-00777-7>.

Correspondence and requests for materials should be addressed to Jianpei Geng or Tetyana Shalomayeva.

Reprints and permission information is available at <http://www.nature.com/reprints>

Publisher's note Springer Nature remains neutral with regard to jurisdictional claims in published maps and institutional affiliations.



Open Access This article is licensed under a Creative Commons Attribution 4.0 International License, which permits use, sharing, adaptation, distribution and reproduction in any medium or format, as long as you give appropriate credit to the original author(s) and the source, provide a link to the Creative Commons license, and indicate if changes were made. The images or other third party material in this article are included in the article's Creative Commons license, unless indicated otherwise in a credit line to the material. If material is not included in the article's Creative Commons license and your intended use is not permitted by statutory regulation or exceeds the permitted use, you will need to obtain permission directly from the copyright holder. To view a copy of this license, visit <http://creativecommons.org/licenses/by/4.0/>.

© The Author(s) 2023